Effects of Vertical Wind Shear on Intensity and Rainfall Asymmetries of Strong Tropical Storm Bilis (2006)

Yu JinHua[1,2], Tan Zhe-Min[1], and Yuqing Wang[3]

1. Key Laboratory of Mesoscale Severe Weather/Ministry of Education, and Department of Atmospheric Sciences, Nanjing University, Nanjing, 210093

2. School of Atmospheric Sciences, Nanjing University of Information Science & Technology, Nanjing, 210044

3 International Pacific Research Center and Department of Meteorology, School of Ocean and Earth Science and Technology, University of Hawaii at Manoa, Honolulu, HI 96822

July 23, 2009

Dateline

Corresponding author address：Dr. Zhe-Min Tan, Department of Atmospheric Sciences, Nanjing University, Nanjing 210093, China. Email: zmtan@nju.edu.cn

Abstract

The effects of environmental vertical wind shear (VWS) on the intensity and rainfall asymmetries in Tropical Storm (TS) Bilis (2006) have been analyzed based on the TRMM/TMI estimated surface rainfall data, the QuikSCAT wind fields, 850-hPa and 200-hPa winds of the NCEP/NCAR reanalysis, the precipitation data at 5-minute intervals from automatic weather stations over mainland China, and the best track data of TS Bilis. The results show that the simultaneous and 6h-lagged correlation coefficients between VWS and storm intensity (the minimum central sea level pressure) are 0.59145 and 0.57438 (P<0.01), respectively. The averaged VWS was found to be about 11 m s^{-1} and thus suppressed the intensification of Bilis. Distribution of precipitation in Bilis was highly asymmetric. The azimuthally averaged rainfall rate in the partial eyewall, however, was smaller than that in a major outer rainband. As the storm intensified, the major rainband showed an unusual outward propagation. The VWS had a great impact on the asymmetric distribution of precipitation. Consistent with previous modeling studies, heavy rainfall generally occurred downshear to downshear-left of the VWS vector both near and outside the eyewall, showing a strong wavenumber-one asymmetry, which was amplified as the VWS increased.

Key words: vertical wind shear, tropical storm, rainfall distribution

1. Introduction

Although the prediction of tropical cyclone (TC) motion has been improved significantly in the last 3 decades (Chen 2002; McAdie et al. 2000), little progress has been made in the prediction of TC intensity and precipitation (Wang and Wu 2004; Lonfat et al. 2004). To improve the prediction skill of TC intensity and precipitation, it is important to understand processes and factors that affect the intensity and precipitation of TCs.

The environmental vertical wind shear (hereafter VWS) is an important dynamical factor affecting TC intensity and precipitation pattern (e.g., Wang and Holland 1996; Jones 2000; Frank and Ritchie 2001; Wang et al. 2004; Zeng et al. 2007, 2008; Yu and Wang 2009). A number of studies have shown that the environmental VWS has a negative effect on the genesis and intensification of TCs, namely, the weak VWS favors the TC intensification, while the strong VWS would cause weakening of TCs (e.g. Gray 1968; Merrill 1988; Frank and Ritchie 2001; Molinari et al. 2000; Wang et al. 2004; Wong and Chan 2004). As a result, the VWS has been used as a predictor in the prediction of TC intensity (Hebert 1976; DeMaria and Kaplan 1994, 1999).

The precipitation structure in TCs is complicated, but can be considered as the sum of the azimuthally averaged axisymmetric component (radial distribution) and the axially asymmetric component (Frank 1977; Burpee and Black 1989). Based on the satellite microwave observations, Rodgers and Adler (1981) analyzed precipitation radial distributions for 21 TCs in the western North Pacific. They found that as a TC intensified, the azimuthally averaged rainfall rate increased but strong asymmetric component might often occur. The rainfall rate was generally largest in the vicinity of the eyewall and decreased radially outward.

There are also differences in the radial distribution among different storms. This is mainly due to the fact that the spatial distribution of precipitation in a TC is not only controlled by its internal dynamics, but also largely affected by its large scale environmental flow (Marks 1985; Burpee and Black 1989).

For the quantitative precipitation forecast (QPF) associated with a TC, the most difficult as well as the most important is to predict the non-axisymmetric pattern in the precipitation distribution. The rainfall varies largely not only in the radial direction but also in different azimuthal directions. We often observed cases with little precipitation in some quadrants, but with heavy precipitation in other quadrants. Results of Lonfat et al. (2004) indicated that on the global average, the heaviest precipitation generally occurs in the front of a TC and the asymmetry in TC precipitation varies with the TC intensity, i.e. the weaker the TC, the more asymmetric the precipitation distribution. Marks (1985) also found that the precipitation occurs much more frequently in the front of a TC than in the rear, with the strongest precipitation located to the right of the TC center. However in some cases, the strongest precipitation could occur in the rear of a TC (Blackwell 2000), which is mainly associated with the effect of VWS (Corbosiero and Molinari 2002, 2003; Chen et al. 2006).

Previous studies have confirmed that the environmental VWS can have a significant effect on the precipitation distribution in TCs. The VWS contributes to the asymmetric pattern in precipitation, with the largest rainfall in the downshear-left quadrant (Willoughby et al. 1984; Wang and Holland 1996; Reasor and Montgomery 2000; Black et al. 2002; Corbosiero and Molinari 2002). Therefore, the environmental VWS affects not only the TC intensity but also spatial distribution of precipitation in TCs. Using the airborne dual Doppler radar

reflectivity data, Reasor et al.(2000) showed that when the environmental VWS increased from 5 m s^{-1} to 15 m s^{-1}, the quasi-axisymmetric distribution in reflectivity of a hurricane involved into an azimuthal wavenumber-one pattern, with strong upward motion occurring downshear of the vertical shear vector and strongest updrafts being downshear left.

Based on the airborne radar data and in-situ observations, Black et al (2002) showed that the VWS contributed a lot to the convective organization and evolution in Hurricanes Jimena (1991) and Olivia (1994) in the eastern Pacific. Convection was organized into an axisymmetric ring as Olivia (1994) intensified in the weak VWS. When the storms experienced stronger VWS, both radar reflectivity and vertical motion displayed a strong wavenumber-one structure. Highest reflectivity generally appeared to the left of the shear vector. Most radar echoes and updrafts formed in the downshear quadrant of the storm and rotated around the storm center at a speed about 60%–80% of the swirling wind. Both the buoyant updrafts and high reflectivity enhanced as they passed through the downshear-left quadrant. Zehr (2003) analyzed the satellite infrared images of Hurricane Bertha (1996) and also confirmed that the weak environmental VWS often corresponds to symmetric distribution in cloud pattern, but the strong shear produces a strong wavenumber-one asymmetric distribution.

Chen et al. (2006) found that the maximum rainfall occurred predominantly downshear left for VWS > 7.5 m s^{-1}. Both the VWS and the TC translation can have significant effects on the asymmetric distribution in TC rainfall, with the VWS being dominant if VWS > 5 m s^{-1}. When the VWS is less than 5 m s^{-1}, the storm translation would contribute equally to the asymmetric distribution in TC rainfall. Cecil (2007) indicated that the rainfall rate in the

downshear-left quadrant can be more than twice of that in other quadrants in the inner core for storms experiencing the VWS greater than 10 m s^{-1}. Beyond 100 km from the storm center, the asymmetry could increase to a factor of four or even larger.

The predominant downshear-left rainfall asymmetry in TCs was first found in Wang and Holland (1996) in a numerical study. Later on, the downshear-left enhancement of rainfall rate for a TC in VWS has been confirmed in more advanced numerical models and in real-case TC simulations (e.g., Bender 1997; Frank and Ritchie 1999, 2001; Rogers et al. 2003). These numerical studies have also investigated the physical mechanisms responsible for the development of convective asymmetries under the VWS effect. It is found that the interaction of a TC with a vertically sheared environmental flow favors the upward motion and low-level convergence downshear of the VWS vector due to the relative flow across the high potential vorticity (PV) core and the requirement of thermal wind balance for the tilted cyclonic circulation (Jones 1995, 2000; Wang and Holland 1996; and Bender 1997). The cyclonic flow advects the asymmetry downstream, resulting in the enhanced upward motion and thus convection downshear-left in the eyewall for a TC embedded in a VWS (see a review by Wang and Wu 2004).

Strong Tropical Storm Bilis (2006) formed at 06 UTC 9 July 2006 in the western North Pacific (centred at 13.4°N, 137°E) and reached its maximum intensity at 12 UTC 12 July with its maximum surface wind speed of 28 m s^{-1}. Although it was a strong tropical storm, Bilis produced heavy rainfall in its lifecycle and brought about severe disasters in South China after its landfall. Both satellite infrared images and rainfall rate estimated from the TRMM/TMI data showed obvious asymmetric distribution in Bilis. A distinct feature is the heavy rainfall

observed far away from the storm center with the largest precipitation occurring to the west and southwest.

During TC landfall, the topography and change in the underlying surface also affect precipitation distribution in addition to the VWS and translational speed. The objective of this study is to examine the physical processes that caused the asymmetric distribution in precipitation in Bilis and focus on analysing the relationship between the VWS and the rainfall distribution of Bilis during its landfall based on a number of data sources. We will show that the northeasterly VWS was responsible for the observed precipitation distribution. In addition, the relationship between the VWS and the storm intensity evolution will also be briefly discussed.

The rest of the paper is organized as follows. Section 2 briefly introduces the data and analysis methods used in this study. The correlation between the VWS and the intensity change of Bilis is presented in section 3. The spatial distribution of precipitation in Bilis and the possible contribution by the VWS to strong rainfall outside the partial eyewall are examined in section 4. Main conclusions are drawn in the last section.

2. Data and methodology

The 850hPa and 200hPa winds and sea level pressure fields from the National Centers for Environmental Prediction(NCEP) final analysis data at a resolution of 1°×1° and at every 6-h intervals during 9-14 July 2006 were used in this study. The method of Paterson et al. (2005) was utilized to calculate the environmental VWS. By this approach, we first did a low-pass filter (Weber and Smith 1995） to the objective analyses. Then a symmetric vortex was removed from the remaining zonal and meridional wind fields to obtain the large-scale

environmental flow which included both the low-pass filter field and the remaining field after the symmetric vortex was removed in the second step. Finally, the environmental VWS vector was calculated as the difference of vector winds between 200 hPa and 850 hPa averaged over an area of 10°×10° centered at the storm center. In addition, the QuikSCAT orbital sea-surface wind fields at the time close to that of the Tropical Rainfall Measuring Mission (TRMM) precipitation estimation on 10 July 2006 were also used to analyze the relationship between the asymmetric surface wind field and the precipitation distribution.

Precipitation data used in this study include observations from the surface automatic weather stations at every 5 minutes from 13 to 15 July 2006 and the surface rainfall estimated from the TRMM/TMI from 9 to 14 July 2006. The ground-based radar reflectivity data were also used in some of our analyses to validate the TRMM/TMI rainfall estimation. We selected 14 samples from TRMM/TMI data for the analysis of precipitation in Bilis. The TRMM satellite has a maximum swath of 760 km with a time resolution of 16 orbits per day and a spatial resolution of 0.1°×0.1°. Note that the storm intensity, position, and VWS at the time of TMI observation were linearly interpolated from their values at the nearest two times.

Generally, the surface precipitation rate over land estimated from TRMM/TMI is weaker than the surface observations (Lonfat et al. 2004). Chen et al. (2006) compared the regional mean rainfall from the surface observation and the estimation from TRMM for 19 TCs before and after landfall. Their results show that both the observed and estimated precipitations have a similar probability density function. To validate the TRMM/TMI rainfall estimation, the TMI estimated precipitation data in the periods of 1256 to 1258 UTC 14 July 2006 (Fig.1b) were compared with the radar reflectivity at 1300 UTC 14 July 2006 from a Taiwan island

radar (Fig.1a). It was found that the large TMI rainfall rate area is consistent with the high radar reflectivity area. The TMI estimated surface rainfall on 14 July 2006 was also compared with the surface rainfall observation from automatic weather stations. It showed that the distribution and heavy precipitation centers from the TMI estimation were generally comparable to the surface observations (not shown). However, some discrepancies existed but were not dramatic. This thus allowed us to use the TRMM/TMI estimated rainfall to study the precipitation structure of Bilis. Note that the discrepancies between the estimated and surface observed rainfall may originate from many aspects, such as the difference in time period, limited spatial resolution of automatic weather stations, narrow swath of the TRMM satellite, complicated topography, and so on.

The wave decomposition algorithm of Yu et al. (2003) was used to calculate the radial and azimuthal distributions of precipitation in Bilis. The longitude and latitude coordinates were transformed into the corresponding polar coordinates (r, θ) with the origin at the center of Bilis determined by linear temporal interpolation. The computational domain in the polar coordinates is a circle with a radius of 852 km. The spatial resolution in the polar coordinates was then set to be Δr = 10.65 km and $\Delta\theta$ =2°, thus having total grid points of 81×181. The TRMM/TMI estimated rainfall rate was decomposed into different wavenumbers in the azimuthal direction at any given radii. The phase and amplitude of each wavenumber component is then calculated and used to discuss the asymmetric structure of precipitation distribution in section 4.

3. Relationship between the VWS and the intensity change of Bilis

Bilis formed in the western North Pacific, centred at (13.4°N, 137°E), at 0600 UTC 9 July 2006 and intensified slowly afterwards as it moved northwestward at a varying translational speed (Fig. 2). It reached its maximum intensity at 0600 UTC 12 July 2006 with the minimum central sea level pressure of 984 hPa and the maximum surface wind speed of 28 m s^{-1}, namely a strong TS, and maintained this intensity until 0300 UTC 14 July. Figure 3 displays the temporal evolution of the Bilis' intensity (the minimum central sea level pressure) and environmental VWS. There is a clear negative correlation between the VWS and the storm intensity. In the early and late stages of the storm's lifecycle, the environmental VWS was mostly above 10 m s^{-1} with the maximum VWS of 15.2 m s^{-1} at 1800 UTC 9 July 2006. In contrast, the VWS was generally below 10 m s^{-1}, with the minimum VWS 4.85 ms^{-1} at 0600 UTC 13 July 2006 when the storm was intensifying. The averaged environmental VWS over the Bilis' lifecycle was about 11 m s^{-1}, which was a little larger than the moderate shear, and thus unfavourable for Bilis to further intensify. The simultaneous and 6h-lagged linear correlation coefficients between the VWS and the central sea level pressure of Bilis were 0.59145 and 0.57438, respectively, significant at the 0.01 confidence level. However, the 12h-lagged linear correlation was not significant even at the 0.10 confidence level. These statistical results are similar to those of the observational analysis by Gallina and Velden (2002) and the numerical simulation by Wong and Chan (2004). Gallina and Velden (2002) found that the critical VWS for the changeover from TC intensification to decay in the Northwest Pacific is about 9-10 m s^{-1}, in agreement with the result of this study. However, Paterson et al. (2005) found that the 36h-lagged correlation coefficient between the VWS and TC intensity change is the most significant for TCs in the Australian region. The difference in

the time lagged correlation between the environmental VWS and TC intensity change from this study and from that of Paterson et al. (2005) might be related to different ocean settings, a topic needs further investigation.

4. Relationship between the VWS and the rainfall distribution in Bilis

Figure 4a shows the surface rainfall rate estimated from the TRMM/TMI during 1323-1326 UTC 10 July when Bilis (2006) reached a maximum surface wind speed of 18 m s^{-1} with its center at (17.0°N, 130.9°E). The environmental flow at that time had a northeasterly shear of 12.9 m s^{-1} (a value slightly larger than a moderate shear). A distinct asymmetric pattern appeared in the precipitation distribution with rainfall largely enhanced downshear to downshear-left of the storm center. The maximum rainfall rate of 24.3 mm h^{-1} occurred at (15.62°N, 130.84°E) about 154 km from the storm center to the left of the VWS. This is in agreement with previous findings on the relationship between the VWS and the precipitation distribution in TCs (Willoughby et al. 1984; Wang and Holland 1996; Reasor and Montgomery 2000; Black et al. 2002; Chen et al. 2006; Cecil 2007).

Corbosiero and Molinari (2002) studied the relationship between the lightning frequency and the distribution of precipitation in Atlantic hurricanes and found that lightning mostly occurred downshear left in the inner core region (within 100 km from the storm center) while downshear right in the outer region (100-300 km). Therefore, the relationship between the VWS and the distribution of precipitation may differ in the inner core (near the eyewall) and in the regions outside the eyewall. Willoughby et al. (1984) termed the rainband near the eyewall as the stationary rainband complex (SBC), which was often located downshear within 80-120 km from the TC center. The SBC generally consists of a major convective

10

precipitation band with convective cells and several secondary non-convective precipitation bands near the TC center. Since flight tracks were limited within 150 km from the TC center, the relationship between the VWS and TC rainbands studied by Willoughby et al. (1984) is primarily applied to the region near the eyewall.

Figure 4b gives the TMI-estimated surface rainfall rate about two days later (1309-1312 UTC 12 July) when Bilis attained its peak intensity with the near surface maximum wind speed of 28 m s^{-1} centered at (21.88°N,124.68°E). The relationship between the VWS and the rainfall asymmetry changed little even after Bilis became stronger and the VWS became weaker. The environmental flow now still had a northeasterly shear (227°) but with a lower value of 7.53 m s^{-1} (a moderate shear). Bilis remained its distinct asymmetric distribution in precipitation with heavy rainfall mainly downshear to downshear-left in the vicinity of the large partial eyewall. The maximum averaged rainfall rate of 32.37 mm h^{-1} occurred downshear about 465 km from the storm center. Therefore, the maximum rainfall rate increased, and shifted outward in comparison with that in the early weak stage of the storm as shown in Fig.4a.

After reaching its peak intensity, Bilis (2006) continued to move northwestward and crossed the Taiwan Island and then made landfall over the Mainland China. After moving inland over Mainland China, Bilis turned to the west and then west-southwest (Fig. 2). Although the land effect was involved, the relationship between the VWS and the asymmetric distribution in Bilis' precipitation showed little change with heavy precipitation downshear left (Fig. 4c). Because of both the land effect and the increase in the northeasterly VWS to 13.8 m s^{-1}, the storm's near surface maximum wind speed was reduced by about 20% with a

value of 23 m s^{-1} at this time. In addition, the storm moved west-southwest at about 10 m s^{-1} during this period, the storm translation might contribute to the enhanced precipitation to the front of the storm. Other possible effect may be due to the orography in south China. Therefore, the rainfall pattern over the land could be a result of the combined effects due to VWS, storm translation, and terrain.

The strong surface winds at 2141 UTC 10 July estimated from the QuikSCAT data occurred mainly to the southwest and about 400 km from the TC center (Fig. 5), while heavy precipitation at 2136 UTC 10 July estimated from the TRMM/TMI data were mainly to the south, slightly downstream of strong surface winds (Fig. 6). Overall, the strong surface winds are highly correlated with the heavy precipitation (active convection), in agreement with the results of Willoughby et al. (1984) and Blackwell (2000). However, the radius of maximum wind of Bilis was extremely large compared to the majority of TCs over the western North Pacific. Furthermore, the eyewall did not develop into a convective ring; rather it displayed a partial eyewall in convection throughout its lifecycle. This may be a result of the weak storm and the effect of moderate to strong environmental VWS. Nevertheless, the relationship between the VWS and the asymmetric distribution in precipitation is basically similar to that observed in most other strong TCs (Corbosiero and Molinari 2002; Chen et al. 2006).

Figure 7a shows the radial distribution of the azimuthally averaged rainfall rate estimated from the TRMM/TMI data during the periods of 1323-1326 UTC 10 July (thin curve) and 1309-1312 UTC 12 July (thick curve), respectively. In the first period, the maximum rainfall rate was 9.5 mm h^{-1} at about 150 km from the TC center, and was mainly contributed by the heavy precipitation in the eyewall. During this period, Bilis was weak and

its eyewall was partial and looked as if a semicircle ring-like rainband (Fig. 4a) with some

weak rainfall occurring in the large eye area. In the second period, Bilis reached its peak

intensity. There were four peaks in the radial distribution of rainfall rate. The first peak had

the maximum rainfall rate of 3.7 mm h^{-1} at 74.6 km radius, which corresponded to the spiral

rainband in the eye region. The second maximum rainfall rate of 8.0 mm h^{-1} occurred at about

170 km from the storm center, which was associated with the semicircle ring-like rainband

within the eyewall. The third maximum of 8.6 mm h^{-1} occurred at about 468.6km, which was

associated with a major spiral rainband outside the eyewall with the heavy rainfall downshear

to downshear-left (Fig. 4b). The last and also the largest rainfall rate was located about 724.2

km from the storm center, where precipitation was not associated with the major downshear

spiral rainband but a semicircle ring-like rainband to the east of the eyewall (Fig. 4b). Now

there was no precipitation near the center of the storm but a weak spiral rainband occurred

inside the partial eyewall.

The radial distribution of precipitation in Bilis was quite different from previous studies.

The analysis of airborne radar reflectivity data by Marks (1985) suggested that near the

eyewall of Hurricane Allen, the reflectivity was strongest with the averaged rainfall rate of

11.3 mm h^{-1}. However, the rainfall rate was only about 1.8 mm h^{-1} over the area outside the

eyewall to the radius of 111 km. Therefore, the rainfall was more than 6 times in the eyewall

than in the region outside the eyewall. Using the radar reflectivity data, Burpee and Black

(1989) analyzed the rainfall rate and its evolution in the eyewall region and in spiral rainbands

within a radius of 75 km when Alica (1983) and Elena (1985) approached US coast. The

results showed that their azimuthally averaged rainfall rates within the eyewall were 5.2 and 6

mm h^{-1} and that in the first rainband outside the eyewall were 2.8 and 3.4 mm h^{-1}, respectively. These studies suggest that rainfall rate in a TC generally reaches a maximum in the eyewall and then quickly decreases outwards. However, the rainfall rate in the partial eyewall of Bilis (2006) is smaller than that in an outer spiral rainband at some stages (Fig. 7a) with strong precipitation occurring in major spiral rainbands even over 400 km from the storm center, suggesting that Bilis was a very special case in the sense of the rainfall structure.

The structure of a TC can be classified into either quasi-axisymmetric or axially asymmetric category. Generally, a strong TC has quasi-axisymmetric structure with convection within 100 km from the TC center and often organized in a strong precipitation ring in the eyewall collocated with the low-level maximum tangential wind. This category TCs can even develop into annular TCs without any major spiral rainbands (Knaff et al. 2005; Wang 2008). The second category TCs have a distinctive asymmetric structure with relatively weaker intensity in general. These storms may be significantly affected by large-scale environmental VWS. In these cases, eyewall convection could not be organized in a closed ring structure but part of a ring, namely, a partial eyewall. In some other cases, strong precipitation occurs mainly in the spiral rainbands outside the eyewall, such as in SBC (Willoughby et al. 1982, 1984; Jorgensen 1984). Obviously, Bilis (2006) belongs to the second category, having a weak intensity with strong precipitation far away from its center.

To further reveal the change in precipitation character during different stages of Bilis, we performed a composite analysis for the radial distribution of azimuthally averaged rainfall rate in two periods, namely, during 9-12 July and 13-14 July, respectively (Fig. 7b). Bilis mainly moved over the ocean during 9-12 July with heavy precipitation very close to its

center. However, during 13-14 July, Bilis (2006) was affected by Taiwan Island, coastal

mountains and land processes over South China as well as the large environmental VWS. As a

result, heavy rainfall occurred several hundred kilometers from the storm center (thin curve in

Fig.7b). Note that due to the narrow swath of TRMM satellite, many instantaneous images of

Bilis used to produce the composite did not cover the Bilis completely. This might affect the

composite results. For example, the radial gradient of rainfall rate across the eyewall could be

reduced when Bilis was at its peak intensity on 12 July.

The spatial distribution of precipitation in Bilis can be decomposed into the

axisymmetric (azimuthal mean) and asymmetric (deviation from the azimuthal mean)

components. The asymmetric component can be further decomposed into different

wavenumber structures. Table 1 lists the amplitudes of wavenumber 1-8 components at radii

74.6, 170.4, 468.6, and 724.2 km, respectively, roughly along the four azimuthally averaged

maximum rainfall rates in Fig. 7a (thick curve for 12 July). Obviously, the amplitude of

wavenumber one is the largest among the first eight wavenumbers at the four radii. The

squared amplitude represents the power. The ratio of the wavenumber-one power to the total

power of the wavenumber 1-8 is 67.43% at 170.4 km, 30.14% at 724.2 km, 27.24% at 468.6

km, and 22.14% at 74.55 km, respectively. The asymmetry in precipitation was the largest

near the eyewall, but weakest inside the eyewall. Similar results apply to the precipitation

distribution on 10 July in Fig. 7a (thin curve). Namely, the amplitude of wavenumber-one

component was the largest at all radii and the ratio of the wavenumber-one power to that of

the total wavenumbers for the largest amplitude at 149 km (near the eyewall) was 76.58%.

5. Conclusions

The TRMM/TMI orbital surface rainfall rate estimations and other relevant data have been used in this study to analyze the relationship between the environmental VWS and the intensity change and precipitation structure of strong Tropical Storm Bilis (2006) in the western North Pacific. The environmental VWS had a statistically close correlation with the intensity change of Bilis. It is found that the linear correlation between VWS and the 6h-lagged storm intensity change is significant at 0.01 confidence level. The overall larger VWS suppressed the further intensification of Bilis. Precipitation in Bilis displayed a distinctive asymmetric structure with the wavenumber-one component dominated and enhanced precipitation downshear to downshear-left of the environmental VWS vector. The asymmetry in the precipitation distribution was shown to be positively correlated with the magnitude of the environmental VWS.

Bilis only reached its peak intensity of 28 m s^{-1} as a strong TS mainly due to the negative effect of a persistent northeasterly VWS throughout its lifecycle. A major feature of Bilis was its large, partial eyewall structure in convection with strong precipitation mostly downshear to downshear-left while little precipitation upshear to upshear right. Furthermore the large precipitation mostly occurred far away from the storm center, thus bearing the common feature of weak TCs embedded in strong environmental VWS. The spatial distribution in precipitation in Bilis was found to be highly correlated with the near-surface strong wind speed, consistent with that found by Willoughby et al. (1984). In addition to the dominant effect of the environmental VWS, the translation of the storm itself, the terrains and the land surface processes may all contribute to some degree to the spatial distribution in precipitation in Bilis.

Although Bilis (2006) is a weak storm compared to many other strong typhoons, such as Supertyphoon Saomai (2006) in the same year in the western North Pacific, it produced heavy rainfall and possessed similar asymmetric precipitation structure before and after landfall. It is however not clear what determined the large size of its eyewall and why the precipitation was so heavy. We consider that the southwesterly monsoon flow and the northeasterly VWS must play some critical roles. It is also an issue about the relative role of the environmental VWS and the storm translation in the case of Bilis. We expect to perform numerical experiments to further address these issues in a future study.

References

Bender, M.A., 1997: The effect of relative flow on the asymmetric structure in the interior of hurricanes. *J. Atmos. Sci.*, **54**, 703-724.

Black, M.L., J.F. Gamache, F.D. Marks Jr., C.E. Samsury, and H.E. Willoughby, 2002: Eastern Pacific hurricanes Jimena of 1991 and Olivia of 1994: The effect of vertical shear on structure and intensity. *Mon. Wea. Rev.,* **130**, 2291-2312.

Blackwell, K.G., 2000: The evolution of hurricane Danny (1997) at landfall: Doppler -observed eyewall replacement, vortex contraction/Intensification, and low-level wind maxima, *Mon. Wea. Rev.,* **128**, 4002-4016.

Burpee, R.W., and M.L. Black, 1989: Temporal and spatial variations of rainfall near the centers of two tropical cyclones, *Mon. Wea. Rev.*, **117**, 2204-2218.

Cecil, D.J., 2007: Satellite-derived rain rates in vertically sheared tropical cyclones, *Geophys. Res. Lett.*, **34**, L02811, doi:10.1029/2006GL027942.

Chen, S.S., J.A. Knaff, and F.D. Marks, Jr., 2006: Effects of vertical wind shear and storm motion on tropical cyclone rainfall asymmetries deduced from TRMM, *Mon. Wea. Rev.*, **134**, 3190-3208.

Chen L.-S., X.-D. Xu, and Z.-X. Luo, 2002: *Introduction to Tropical Cyclone Dynamics.* China Meteorological Press, Beijing, 300pp.

Cheng M.-H., 2006: *The Studies of Landfalling Tropical Cyclone Using TRMM and HK Radar Data,* Team member report on topic 0.3 of IWTC-Ⅵ.

Corbosiero, K.L., and J. Molinari, 2002: The effects of vertical wind shear on the distribution of convection in tropical cyclones. *Mon. Wea. Rev.,* **130,** 2110-2123.

Corbosiero, K.L., and J. Molinari, 2003: The relationship between storm motion, vertical

wind shear and convective asymmetries in tropical cyclones, *J. Atmos. Sci.*, **60,** 366-376.

DeMaria, M., and J. Kaplan, 1994: Statistical hurricane intensity prediction scheme (SHIPS) for the Atlantic basin, *Wea. Forecasting,* **9**, 209-220.

DeMaria, M., 1996: The effect of vertical shear on tropical cyclone intensity change, *J. Atmos. Sci.*, **53,** 2076-2087.

DeMaria, M., and J. Kaplan, 1999: An updated statistical hurricane intensity prediction scheme (SHIPS) for the Atlantic and eastern north Pacific basins. *Wea. Forecasting*, **14,** 326-337.

Frank, W.M., 1977: The structure and energetics of the tropical cyclone, Part Ⅰ: Storm structure, *Mon. Wea. Rev.,* **105**, 1119-1125.

Frank, W.M., and E.A. Ritchie, 1999: Effects of environmental flow upon tropical cyclone structure. *Mon. Wea. Rev.,* **127**, 2044-2061.

Frank, W.M., and E.A. Ritchie, 2001: Effects of vertical wind shear on hurricane intensity and structure. *Mon. Wea. Rev.,* **129,** 2249-2269.

Gallina, G.M., and C.S. Velden, 2002: Environmental vertical wind shear and tropical cyclone intensity change utilizing enhanced satellite derived wind information. *Proceedings of the 25th Conference on Hurricanes and Tropical Meteorology, 29 April - 3 May 2002, San Diego, CA.* pp172-173.

Gray, W.M., 1968: Global view of the origin of tropical disturbances and storms. *Mon. Wea. Rev.*, **96**, 669~700.

Hebert, P.J., 1976: Intensification criteria for tropical depressions of the western

hurricane-Inez (1966). *Mon. Wea. Rev.*, **104**, 418-442.

Jones, S.C., 1995: The evolution of vortices in vertical shear, I: initially barotropic vortices. *Quart. J. Roy. Meteor. Soc.*, **121**, 821-851.

Jones, S.C., 2000: The evolution of vortices in vertical shear, II: initially baroclinic vortices. *Quart. J. Roy. Meteor. Soc.*, **126**, 3161-3185.

Jorgensen, D.P., 1984: Mesoscale and convective scale characteristics of mature hurricanes, Part I: General observations by research aircraft. *J. Atmos. Sci.*, **41**, 1268-1285.

Knaff, J.A., C.R. Sampson, and M. DeMaria, 2005: An operational statistical typhoon intensity prediction scheme for the Western North Pacific. *Wea. Forecasting,* **20**, 688–699.

Kummerow, C., W. Barnes, T. Kozu , J. Shiue, and J. Simpson, 1996: The tropical rainfall measuring mission(TRMM) sensor package, *J. Atmos. Ocea. Technol.,* **15**, 809-817.

Lonfat, M., F.D. Marks, and S.S. Chen, 2004: Precipitation distribution in tropical cyclones using the tropical rainfall measuring mission (TRMM) microwave imager: A global perspective. *Mon. Wea. Rev.*, **132**, 1645-1660.

Luo Z.-X., 1991: Possible causes of counterclockwise loop of tropical cyclones. *Science in China* (B), **35**, 769-775.

Marks, F.D., Jr, 1985: Evolution of the structure of precipitation in Hurricane Allen (1980), *Mon. Wea. Rev.*, **113,** 909-930.

McAdie, C.J., and M.B. Lawrence, 2000: Improvements in tropical cyclone track forecasting in the Atlantic Basin, 1970-98. *Bull. Amer. Meteor. Soc.,* **81**, 989-998.

Merrill, R.T., 1988: Environmental influences on hurricane intensification. *J. Atmos. Sci.*, **45**, 1678-1687.

Molinari, J., D. Vollaro, and S. Sbubis, 2000: Origins and mechanism of Eastern Pacific tropical cyclogenesis: A case study, *Mon. Wea. Rev.*, **128**, 125-139.

Paterson L.A., B.N. Hanstrum, and N.E. Davidson, 2005: Influence of environmental vertical wind shear on the intensity of hurricane-strength tropical cyclones in the Australian region, *Mon. Wea. Rev.,* **133,** 3644-3660.

Reasor, P.D., M.T. Montgomery, F. D. Marks Jr. and J. F. Gamache, 2000: Low wave structure and evolution of the hurricane inner core observed by airborne and dual-Doppler radar, *Mon. Wea. Rev.*, **128**, 1653-1680.

Rodgers, E.B., and E.F. Adler, 1981: Tropical cyclone rainfall characteristics as determined from a satellite passive microwave radiometer. *Mon. Wea. Rev.*, **109**, 506-521.

Rogers, R., S.S. Chen, and J. Tenerelli, 2003: A numerical study of the impact of vertical shear on the distribution of rainfall in hurricane Bonnie (1998). *Mon. Wea. Rev*, **131,** 1577-1599.

Wang, Y., and G.J. Holland, 1996: Tropical cyclone motion and evolution in vertical shear. *J. Atmos. Sci.*, **53**, 3313-3332.

Wang, Y., and C.-C., Wu, 2004: Current understanding of tropical cyclone structure and intensity changes – a review, *Meter. Atmos. Phys.,* **87**, 257-278.

Wang, Y., M.T. Montgomery, and B. Wang, 2004: How much vertical shear can a tropical cyclone resist? *Bull. Amer. Meteor. Soc.*, **85,** 661-662.

Wang, Y., 2008: Structure and formation of an annular hurricane simulated in a fully-compressible, nonhydrostatic model - TCM4, *J. Atmos. Sci.*, **65**, 1505-1527.

Weber, H.C., and R.K. Smith, 1995: Data sparsity and the tropical-cyclone analysis and prediction problem: Some simulation experiments with a barotropic numerical model. *Quart. J .Roy. Meteor. Soc.*, **121**, 631-654.

William M.F., and A.R., Elizabeth, 2001: Effects of vertical wind shear on the intensity and structure of numerically simulated hurricanes. *Mon. Wea. Rev.*, **129,** 2249-2269.

Willoughby, H.E., J.A. Clos, and M.G. Shoreibah, 1982: Concentric eyewalls, secondary wind maxima and the evolution of the hurricane vortex. *J. Atmos. Sci.*, **39**, 395-411.

Willoughby, H.E., F.D. Marks, Jr., and R.J. Feinberg, 1984: Stationary and moving convective bands in hurricanes. *J. Atmos. Sci.*, **41**, 3189–3211.

Wong, M.L.M., and J.C.L. Chan, 2004: Tropical cyclone intensity in vertical wind shear. *J. Atmos. Sci.*, **61**, 1859–1876.

Yu, J.-H., X.-D. Xu, L.-S. Chen, and Z.-X. Luo, 2003: A numerical study on vorticity propagation and changes in typhoon intensity. *Acta Meteor. Sinica*, **17**, 129-145.

Yu, J.-H., and Y. Wang, 2009: Response of tropical cyclone potential intensity over the north Indian Ocean to global warming, *Geophys. Res. Lett.*, **36**, L03709, doi:10.1029/2008GL036742.

Zeng, Z.-H., Y. Wang, and C.-C. Wu, 2007: Environmental dynamical control of tropical cyclone intensity-An observational study. *Mon. Wea. Rev.*, **135**, 38-59.

Zeng, Z.-H., L.-S. Chen, and Y. Wang, 2008: An observational study of environmental dynamical control of tropical cyclone intensity in the North Atlantic. *Mon. Wea. Rev.*, **136**, 3307–3322.

Zehr, R.M., 2003: Environmental vertical wind shear with Hurricane Bertha (1996). *Wea. Forecasting,* **18**, 345-356.
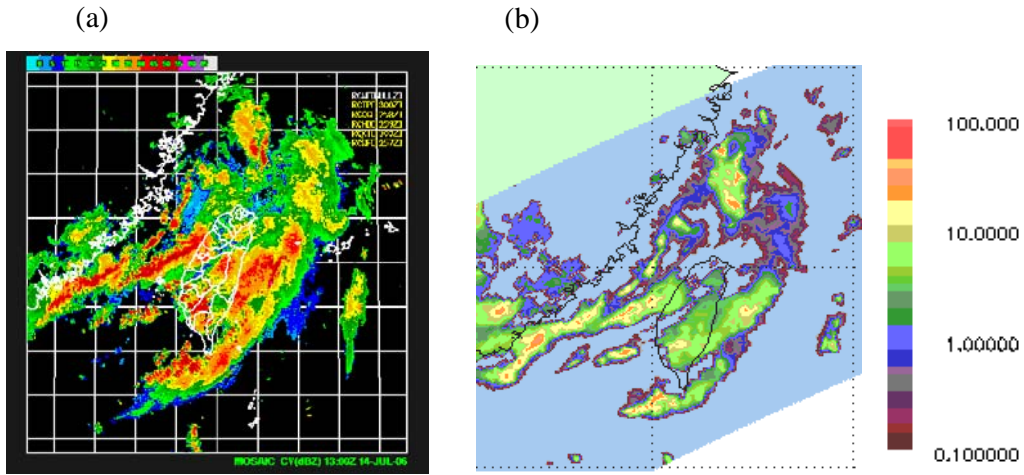
Figure Caption

Fig.1 Comparison between radar reflectivity in Taiwan Island (a, dBZ) and TRMM surface rainfall rate (b, mm h^{-1}) at about 1300 UTC 14 July 2006.
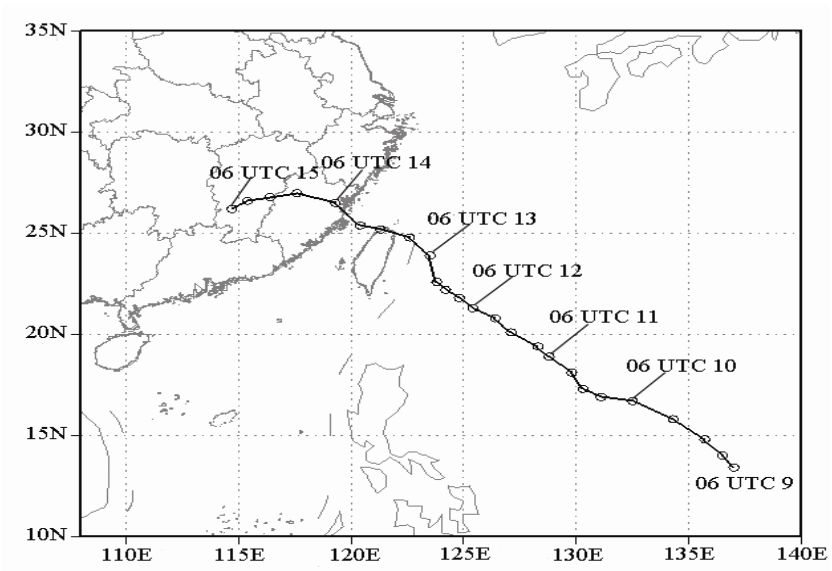
Fig.2. The best track of western North Pacific Tropical Storm Bilis (2006). The open circles denote the positions of Bilis (2006) at 6-h intervals, with the position at 0006 UTC on each day indicated.

Fig. 3. Temporal evolution of the environmental vertical wind shear (VWS) (m s^{-1}, solid) and the surface central pressure of Bilis (2006) (hPa, dashed).

Fig. 4. TRMM/TMI estimated surface precipitation rate (mm h^{-1}). The solid arrow denotes the VWS direction, the dashed arrow indicates the motion direction of the storm. (a) 1323-1326 UTC 10 July 2006, (b) 1309-1312 UTC 12 July 2006, (c) 1927-1930 UTC 14 July 2006.

Fig. 5. The QuikSCAT wind field of Bilis (2006) at 2141 UTC 10 July 2006. The TC symbol marks the position of Bilis (2006) at（17.78°N, 130°E). (a) horizontal wind vector, (b) horizontal wind speed.

Fig. 6. Same as Fig. 3 but for 2135-2138 UTC 10 July 2006.

Fig. 7. The radial distribution of the azimuthally averaged rainfall rate in Bilis (2006) (mm h^{-1}). (a) The thin curve is for 1323-1326 UTC 10 July 2006 (Fig. 3a), and the thick curve is for 1209-1312 12 July 2006 (Fig.3b); (b) the thick curve is for 9-12 July 2006, and the thin curve is for 13-14 July 2006.

Table 1. Amplitudes (mm h^{-1}）of wavenumber (WN) 1-8 components in rainfall rate at 2135-2138 UTC 10 July 2006 along the four radii at 74.5, 170.4, 468.6, and 724.2 km, respectively, where the azimuthally averaged maximum rainfall rates appeared in Fig. 6a (thick curve)

WN / Km	1	2	3	4	5	6	7	8
74.55	1.736	1.66	1.569	1.385	1.186	1.007	0.8	0.635
170.4	6.601	2.672	1.705	1.769	1.46	1.894	1.409	0.413
468.6	4.499	3.761	3.406	2.913	2.844	2.436	1.78	1.623
724.2	5.863	5.386	4.637	2.292	2.011	2.75	2.413	2.546

Fig.1 Comparison between radar reflectivity in Taiwan Island (a, dBZ) and TRMM surface rainfall rate (b, mm h^{-1}) at about 1300 UTC 14 July 2006

Fig.2. The best track of western North Pacific Tropical Storm Bilis (2006). The open circles denote the positions of Bilis at 6-h intervals, with the position at 0006 UTC on each day indicated.
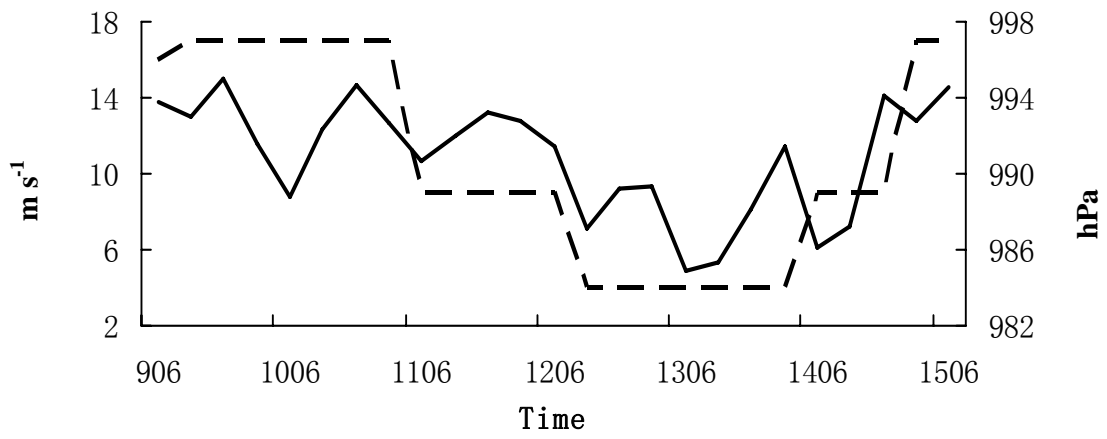
Fig. 3. Temporal evolution of the environmental vertical wind shear (VWS) (ms⁻¹, solid) and the surface central pressure of Bilis (2006) (hPa, dashed).
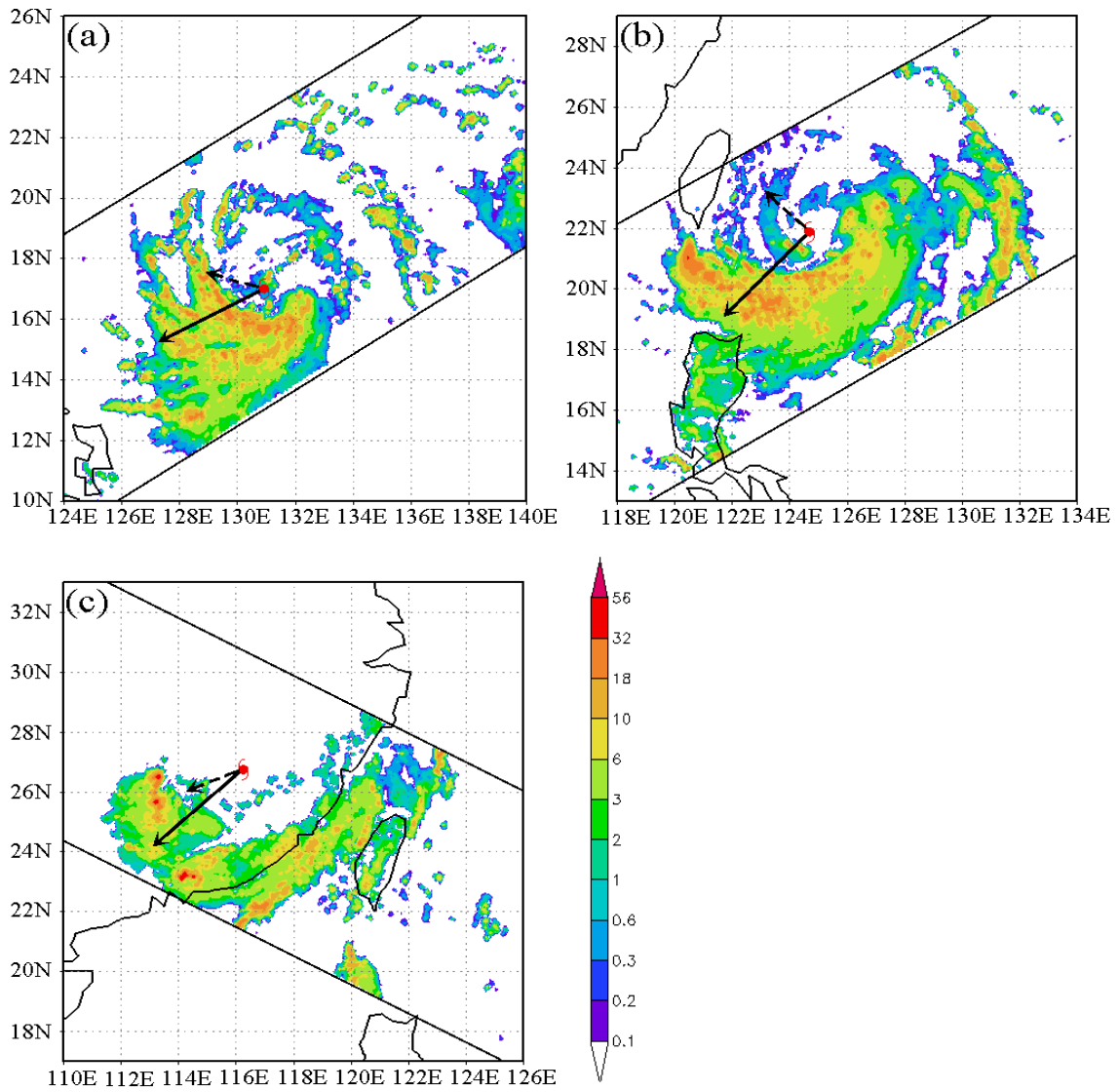
Fig.4. TRMM/TMI estimated surface rainfall rate (mm h^{-1}). The solid arrow denotes the VWS direction, the dashed arrow indicates the motion direction of the storm. (a) 1323-1326 UTC 10 July 2006, (b) 1309-1312 UTC 12 July 2006, (c) 1927-1930 UTC 14 July 2006.
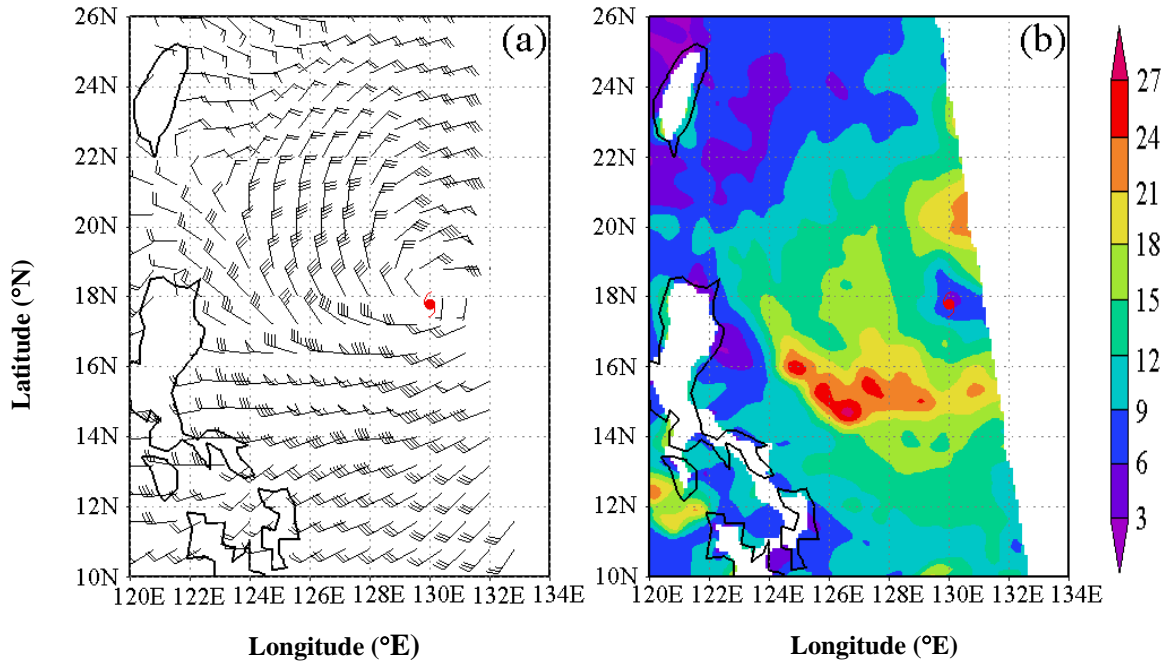
Fig. 5. The QuikSCAT wind field of Bilis (2006) at 2141 UTC 10 July 2006. The TC symbol marks the position of Bilis (2006) at（17.78°N, 130°E). (a) horizontal wind vector, (b) horizontal wind speed.
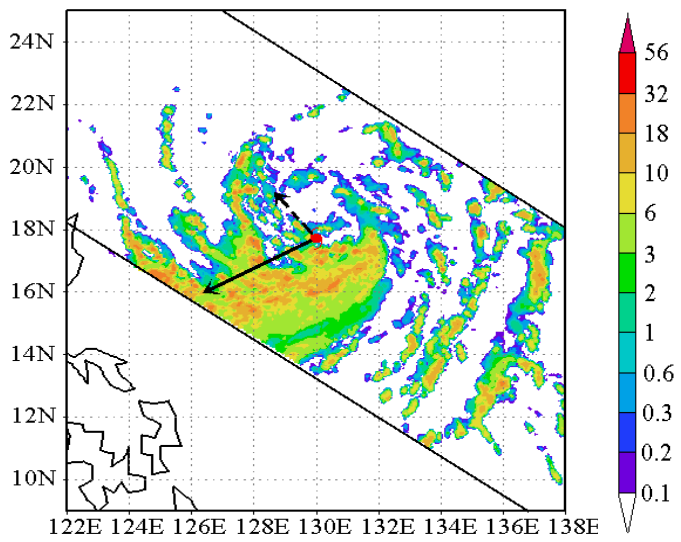
Fig. 6. Same as Fig. 4 but for 2135-2138 UTC 10 July 2006.

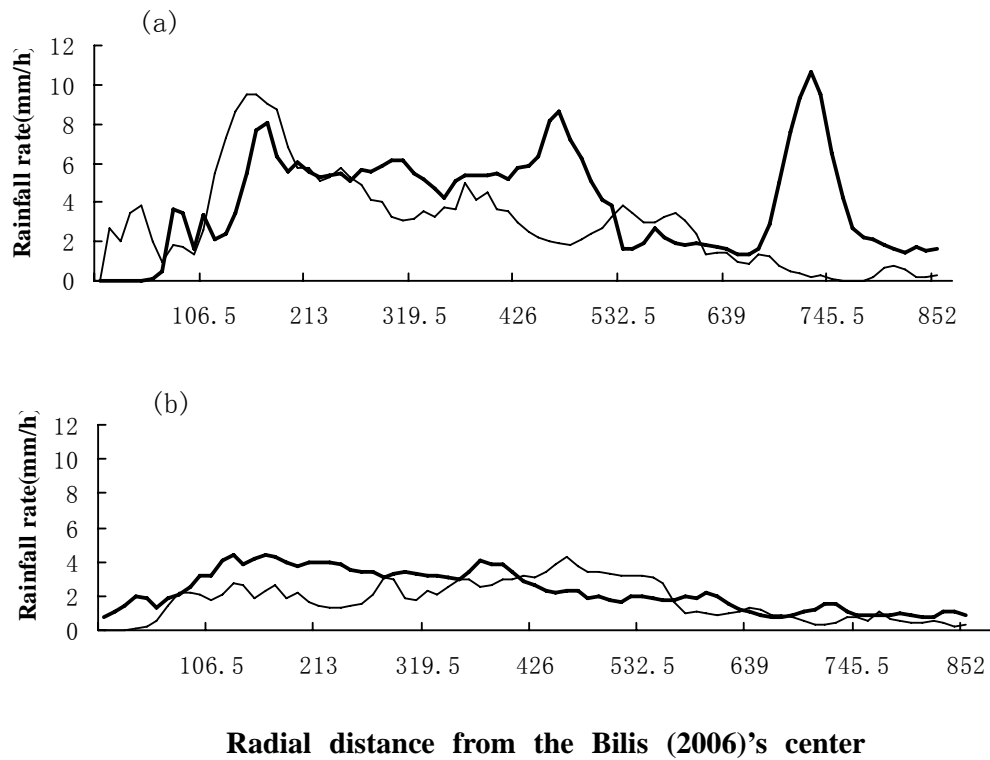**Radial distance from the Bilis (2006)'s center**

Fig. 7. The radial distributions of the azimuthally averaged rainfall rate in Bilis (2006) (mm h^{-1}). (a) The thin curve is for 1323-1326 UTC 10 July 2006 (Fig. 3a), and the thick curve is for 1209-1312 12 July 2006 (Fig.3b); (b) The thick curve is for 9-12 July 2006, and the thin curve is for 13-14 July 2006.